Table of content

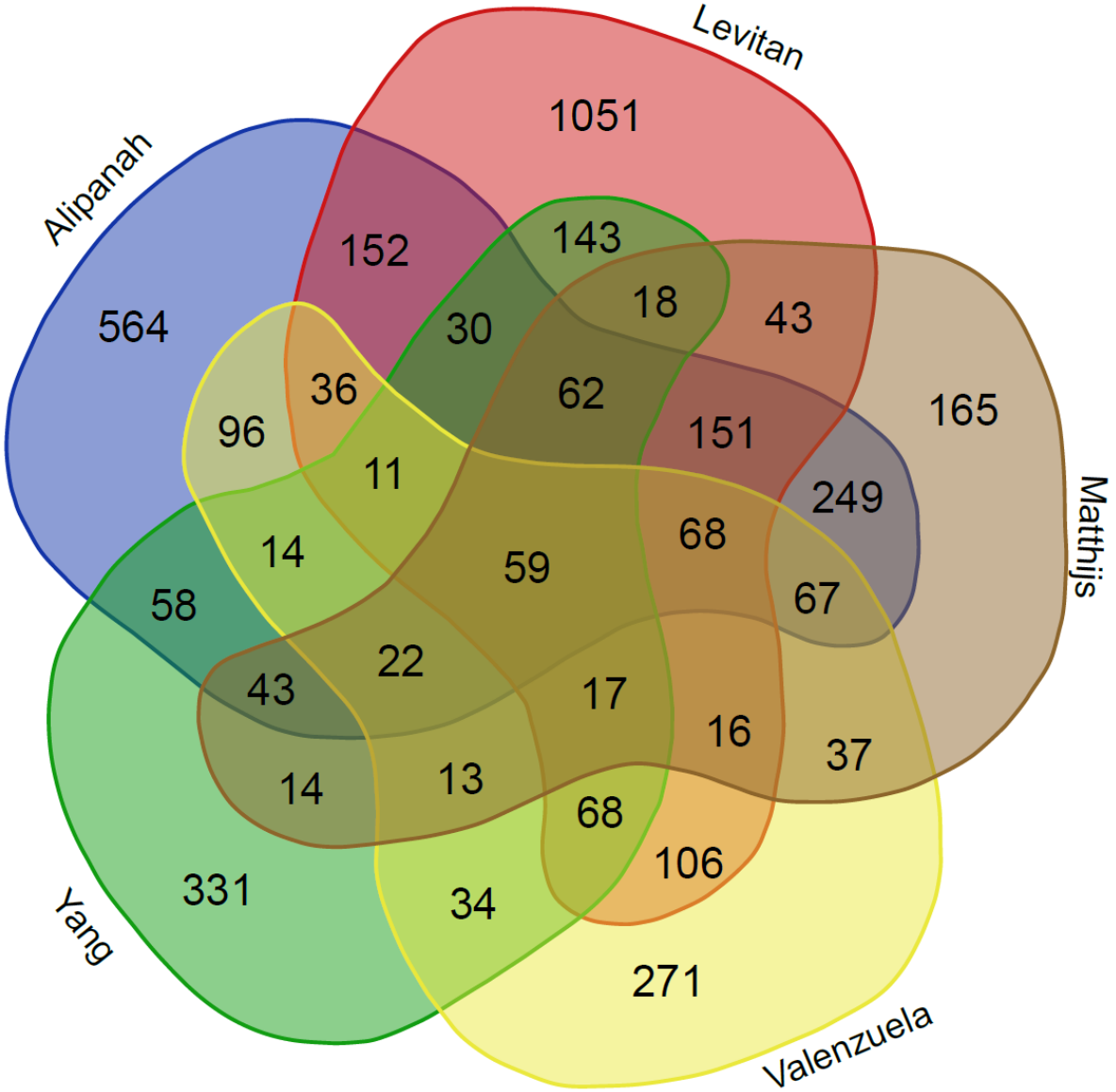

Appendix Figure S1. Overlap between different nitrogen-starvation transcriptome datasets. A cut-off value of 1 $\log_2$ fold upregulation relative to the relevant control in each study was used. Names refer to the respective published studies: Levitan *et al* (2015), Valenzuela *et al* (2012), Yang *et al* (2013), Alipanah *et al* (2015), and Matthijs *et al* (2016).

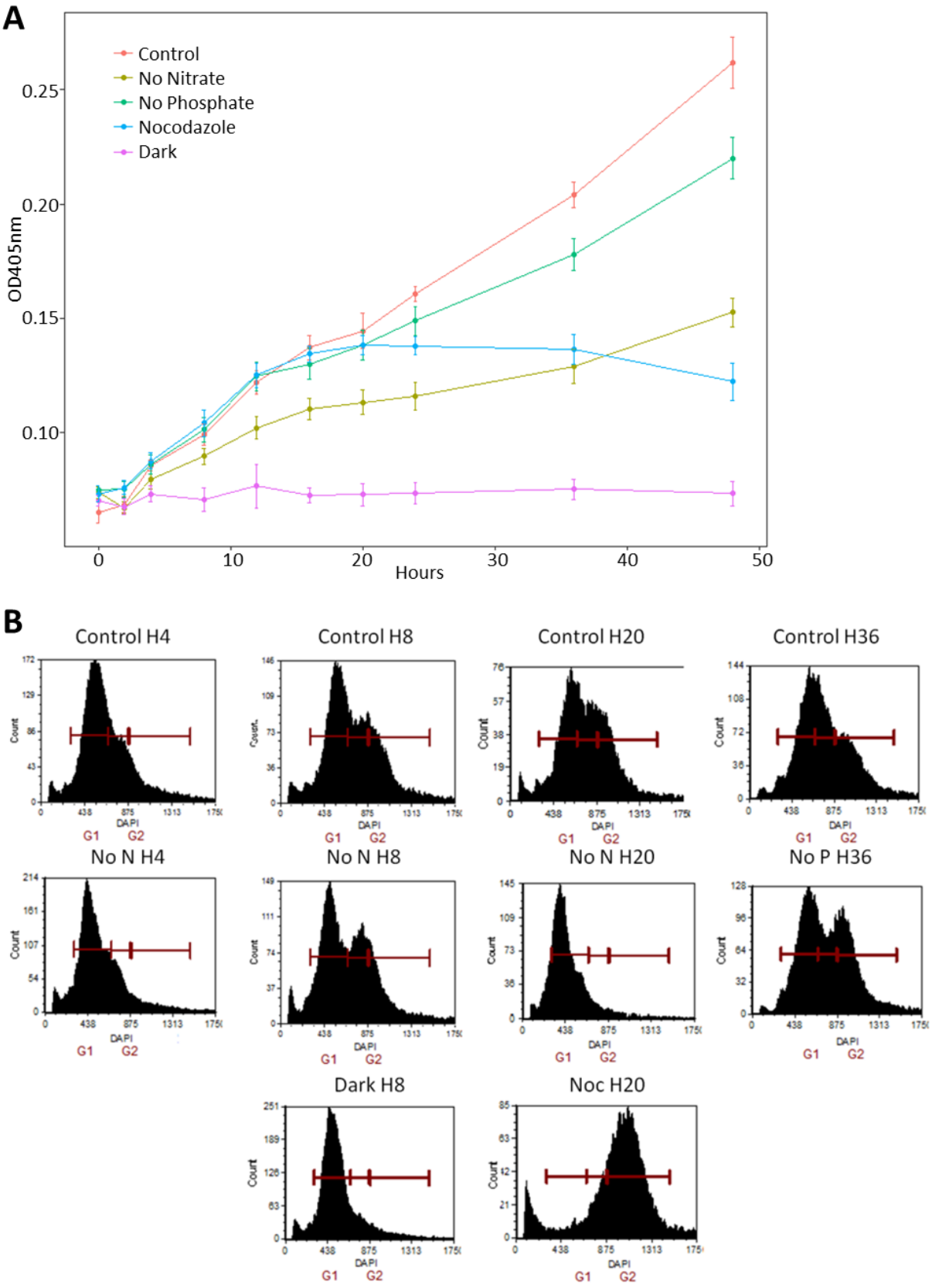
A
Control
No Nitrate
No Phosphate
Nocodazole
Dark
OD405nm
0.25
0.20
0.15
0.10
0
10
20
30
40
50
Hours
B
Control H4
Control H8
Control H20
Control H36
No N H4
No N H8
No N H20
No P H36
Dark H8
Noc H20
Count
DAPI
G1
G2

Appendix Figure S2. Nitrogen starvation and other stresses halt *P. tricornutum* growth and cell cycle progression.

A Relative growth profiles. Growth was measured by OD_{405} (*y*-axis) to show the general trend of growth (n=3). The *x*-axis indicates time in hours. Error bars represent the standard deviation.

B Flow cytometry on DAPI-stained nuclei. Representative flow histogrammes of the samples harvested for RNA-Seq (n=3). 2C and 4C DNA contents correspond with G1 and G2, respectively. The *y*-axis represents the cell counts. The gradual progression from exponential growth towards cell cycle arrest is visible for all treated samples after 8 h (H8), i.e. for nitrogen-starved (No N), dark-incubated (Dark), and nocodazole-treated (Noc) cells, but not for phosphate starved (No P) cells. Nitrogen-starved cells still underwent approximately one more division, but halted their cell cycle at the G1/S transition as illustrated by a decreasing peak at 4C and an increasingly sharp peak at 2C. The cells incubated in the dark showed no increase in culture density (OD), although the flow histogrammes revealed progression of the G2/M phase to G1/S arrest. This apparent contradiction is the consequence of measuring cells by OD only, because it has been shown that cells dividing in the dark have a smaller volume (Chauton *et al*, 2013). The toxic effect of nocodazole was increasingly visible from 20 h onwards, with cells no longer surviving after 48 h, which corresponded to the flow histogrammes, because almost the entire population was in G2/M arrest. The effects of phosphate starvation were very mild compared with the other experimental treatments; however this was anticipated, because the amount of phosphate required for diatom growth is 1/16 of that of nitrogen, as determined by the classic Redfield ratio and cells often contain substantial intracellular stores of this nutrient (Falkowski *et al*, 2004).

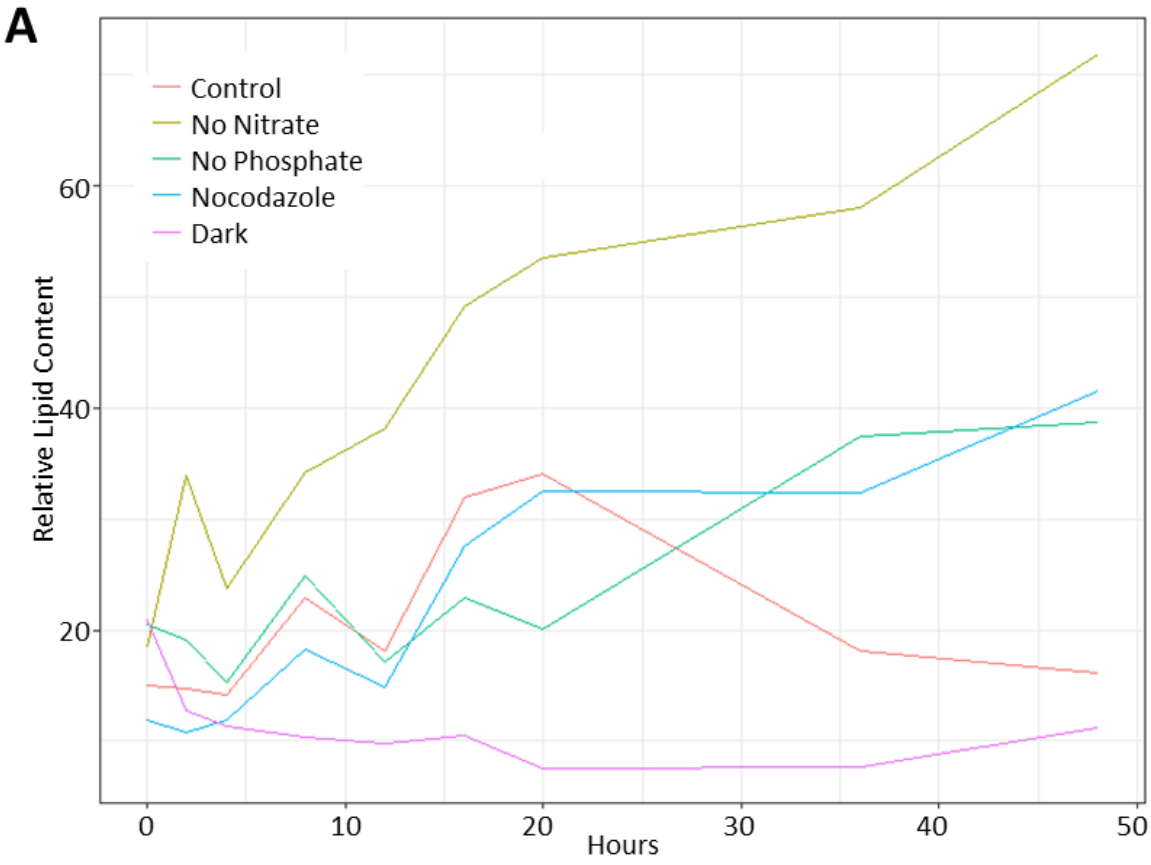
A
Control
No Nitrate
No Phosphate
Nocodazole
Dark
Relative Lipid Content
60
40
20
0
10
20
30
40
50
Hours

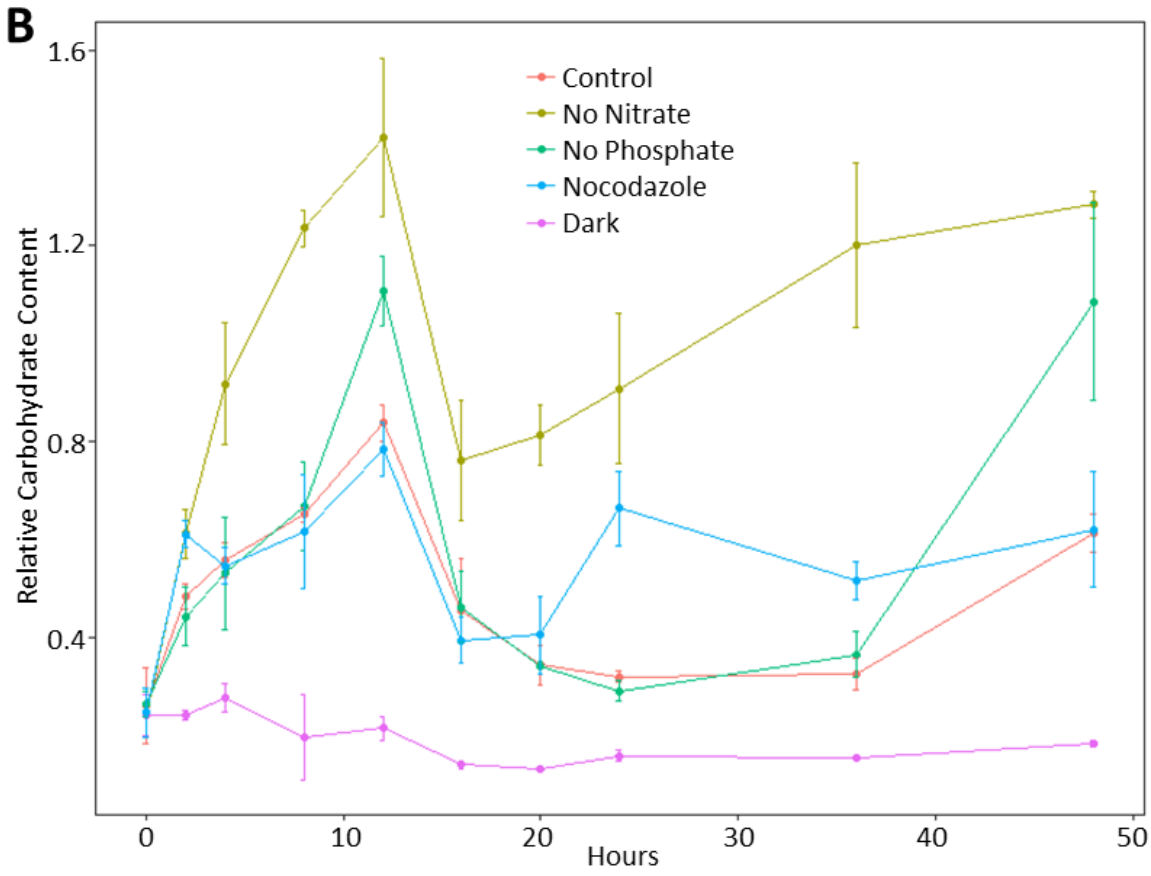
B
Control
No Nitrate
No Phosphate
Nocodazole
Dark
Relative Carbohydrate Content
1.6
1.2
0.8
0.4
0
10
20
30
40
50
Hours

Appendix Figure S3. Nitrogen starvation and other stresses differentially affect lipid and carbohydrate accumulation in *P. tricornutum* cells.

A Lipid content per cell. The *y*-axis represents fatty acid peak area divided by the OD_{405} to account for differences in cell density (n=1). The *x*-axis indicates time in hours. Although the accumulation of lipids in stationary cells during nitrogen starvation is well established, it was not known whether lipid levels would noticeably increase during the shorter time span of our experiments. An unexpected rapid onset of lipid accumulation was visible in nitrogen-deprived cells, already 2 h after medium change. Conversely, cells placed in darkness rapidly consumed the limited amount of lipids stored during the early time points. Phosphate starvation and nocodazole treatment did not profoundly alter the intracellular lipid content compared with the control samples within the first 20 h, and increased lipid accumulation was only apparent after 48 h.

B Soluble carbohydrate content per culture. The *y*-axis represents the measured OD_{495} of phenol-sulphuric acid derivatized sugar extractions (n=3). Error bars represent the standard deviation. The *x*-axis indicates time in hours. The main storage carbohydrate in *P. tricornutum* is chrysolaminarin but the method used cannot discriminate between polysaccharides and monosaccharides. Carbohydrate levels in nocodazole-treated samples were similar to the control. In the three other conditions, carbohydrate and lipid accumulation occurred concurrently. Cells incubated in the dark rapidly consumed their available carbohydrate reserves. Phosphate-starved cells behaved very similarly to the control, but an increased carbohydrate accumulation relative to nutrient-replete cells could be observed after 48 h. In nitrogen-starved cells, carbohydrate levels increased simultaneously with the accumulation of lipids. Although this result differs from a previous profiling study (Valenzuela *et al*, 2012), it is in agreement with the finding that knocking out the committed step of polysaccharide biosynthesis increases lipid accumulation, suggesting a significant carbon flux increase towards carbohydrates under nitrogen-limiting conditions (Daboussi *et al*, 2014). Cells starved for nitrogen during 72 h were previously reported to have increased carbohydrate levels although several enzymes for chrysolaminarin degradation were upregulated (Alipanah *et al*, 2015).

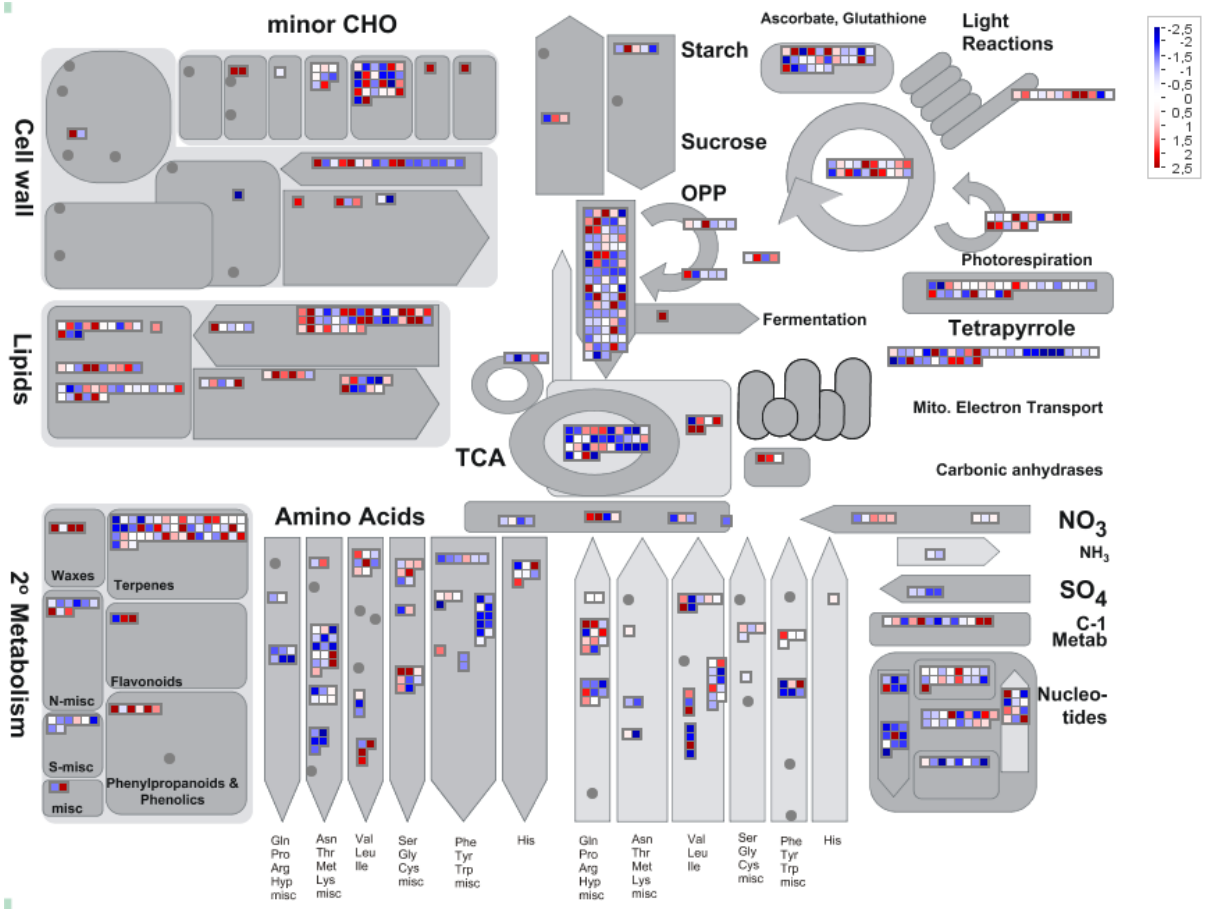

Appendix Figure S4. Effects of dark incubation on the *P. tricornutum* transcriptome. Overview of reprogramming of primary metabolism as visualized by the MapMan programme and using the normalized RNA-Seq data. Points represent the $\log_2$ fold change in gene expression versus control cells at the same time point during incubation in the dark for 8 h (n=3). Red and blue indicate gene induction and repression, respectively. It was our intention to halt lipid accumulation in diatom cells by depriving them of light, thus inhibiting photosynthesis. It should be noted, however, that sample harvesting included filtering, during which exposure of the dark-incubated cells to light for a few minutes was unavoidable. Consequently, these samples may better be considered as re-illuminated rather than strictly dark-incubated samples. A good indicator of this was the upregulation of *dsCyclin2*, a gene which has been reported to rapidly respond to light (Huysman *et al*, 2013), in the 'dark' samples. The light-dark shift resulted in a massive transcriptome change and was thereby the most disruptive treatment in our dataset. The number of up- and downregulated genes was 1,415 and 2,098, respectively (Dataset EV1). In total 120 TFs, over half of all predicted *P. tricornutum* TFs, displayed maximal expression in this sample. A myriad of cellular processes seemed to be affected, which, together with the upregulation of genes related to the photosynthetic machinery, chlorophyll biosynthesis and chloroplast control, points to a general response to light deprivation.

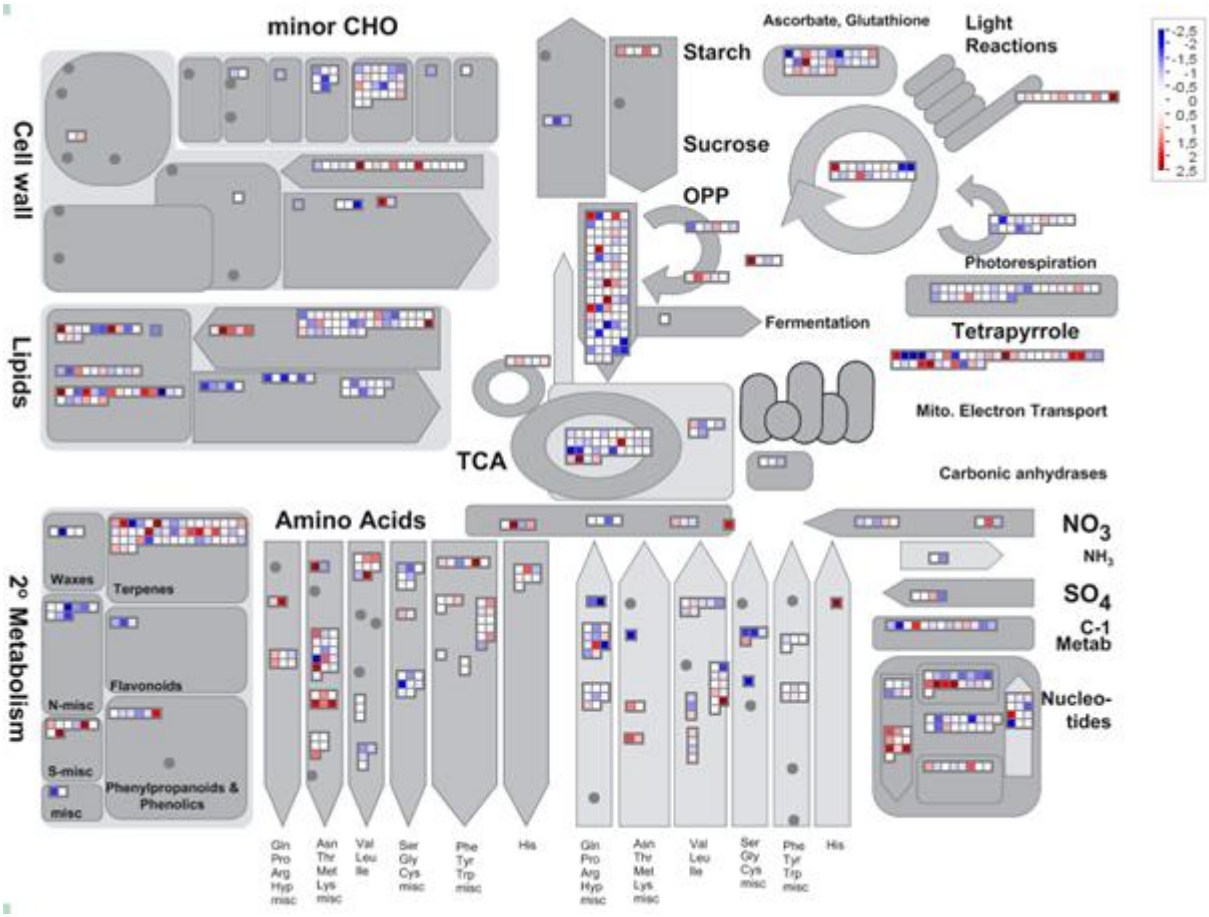

Appendix Figure S5. Effects of nocodazole on the *P. tricornutum* transcriptome. Overview of reprogramming of primary metabolism as visualized by the MapMan programme and using the normalized RNA-Seq data. Points represent the $\log_2$ fold change in gene expression versus control cells at the same time point during a 20-h nocodazole treatment (n=3). Red and blue indicate gene induction and repression, respectively. After 20 h of incubation with nocodazole, 965 and 398 genes were up- and downregulated (Dataset EV1), respectively. Although silicon transporters were amongst the most strongly induced genes, nutrient uptake was generally repressed. The most obvious effect of nocodazole treatment was a G2/M cell cycle arrest.

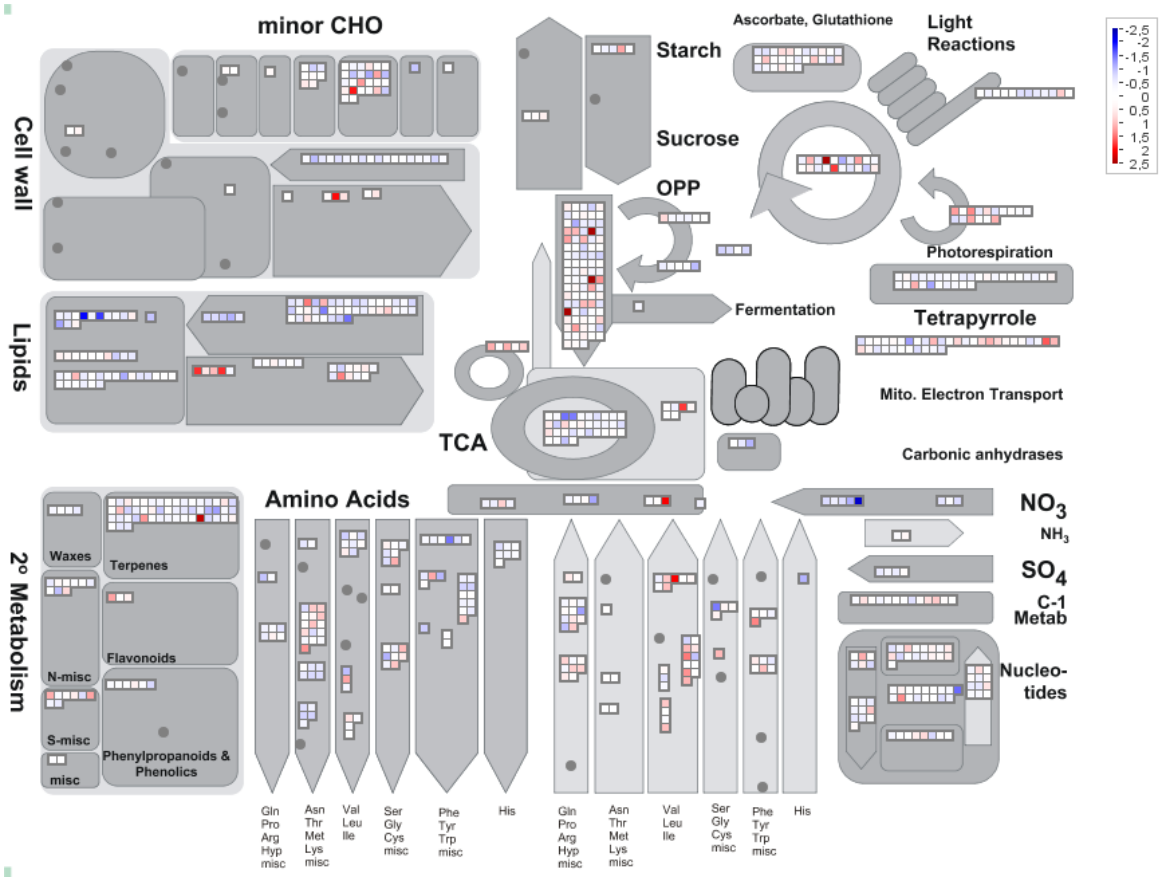

Appendix Figure S6. Effects of phosphorus starvation on the *P. tricornutum* transcriptome. Overview of reprogramming of primary metabolism as visualized by the MapMan programme and using the normalized RNA-Seq data. Points represent the $\log_2$ fold change in gene expression versus control cells at the same time point during a 36-h phosphorus starvation (n=3). Red and blue indicate gene induction and repression, respectively. In agreement with its physiological effects, phosphate starvation had the mildest effects of all stresses as assessed at the transcriptomic level: only 681 genes showed markedly differential expression when compared with the control at 36 h. It seems likely that in our culturing conditions, the cells maintained a large internal pool of stored phosphate and that large-scale changes in cytosolic phosphate occurred only following the depletion of the vacuolar phosphate reserves. This assumption was supported by the observation that cells retained in phosphate-free medium halted growing after 72 h, whereas control samples maintained growth (data not shown). Nonetheless, a typical increase in the uptake capacity for this limiting nutrient and the use of alternative phosphorous sources was apparent in the transcriptome of the phosphate-starved cells, indicating the onset of a specific nutrient stress response in the 36-h sample. Genes encoding phosphate transporters and sodium/phosphate antiporters increased in expression and formed a co-expression cluster with genes coding for several nucleoside phosphatases (Appendix Figure S7), the latter being in close agreement with the role of nucleotides as a storage pool of phosphate. Several genes involved in the creatine cycle, such as creatine kinase and creatine transporters, were strongly downregulated. This pathway is able to rapidly regenerate ATP from ADP, transferring a phosphate group from phosphocreatine. Notably, several genes that were severely downregulated during phosphate starvation were highly upregulated during nitrogen starvation, including the aforementioned creatine transporters.

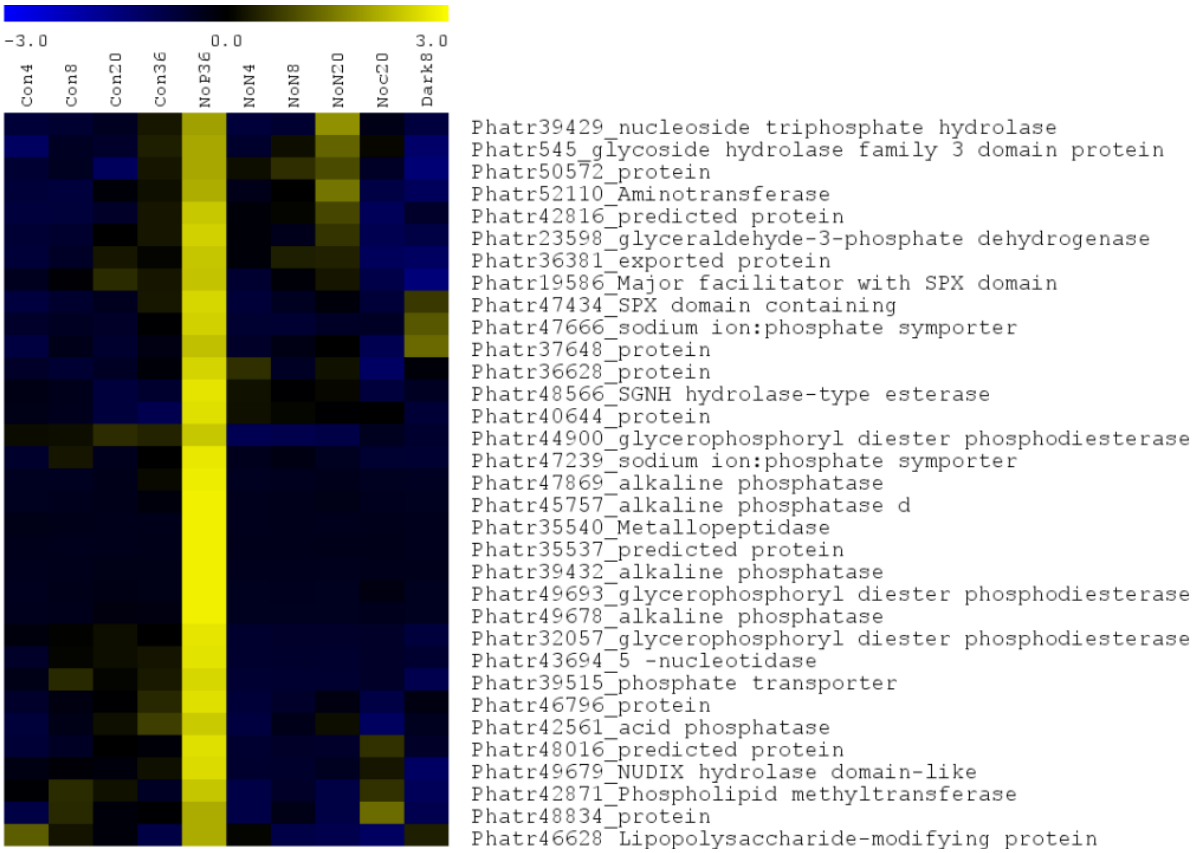

Appendix Figure S7. The phosphate stress cluster. Cluster analysis was performed based on FPKM values normalized to the average FPKM value across all samples. Yellow and blue indicate gene induction and repression, respectively.

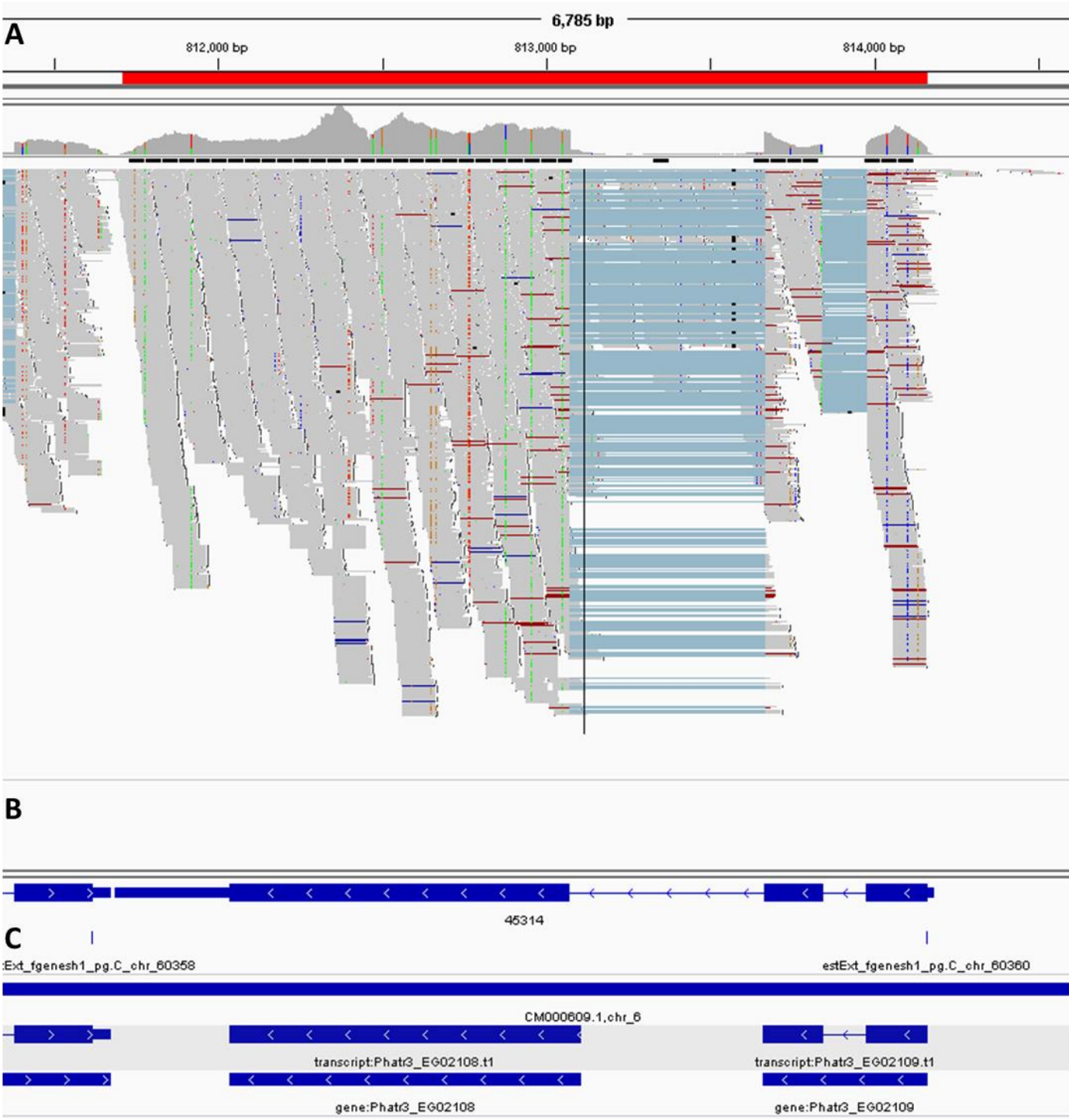

Appendix Figure S8. Comparison of the *Phatr2* and *Phatr3* gene models for *bZIP14*. Screenshot of the alignment of the RNA-Seq reads (A) from the control condition at 20 h with the gene models from the *Phatr2* annotation shown as 45314 (B) and the split gene model from *Phatr3* shown as EG02108 and EG02109 (C).

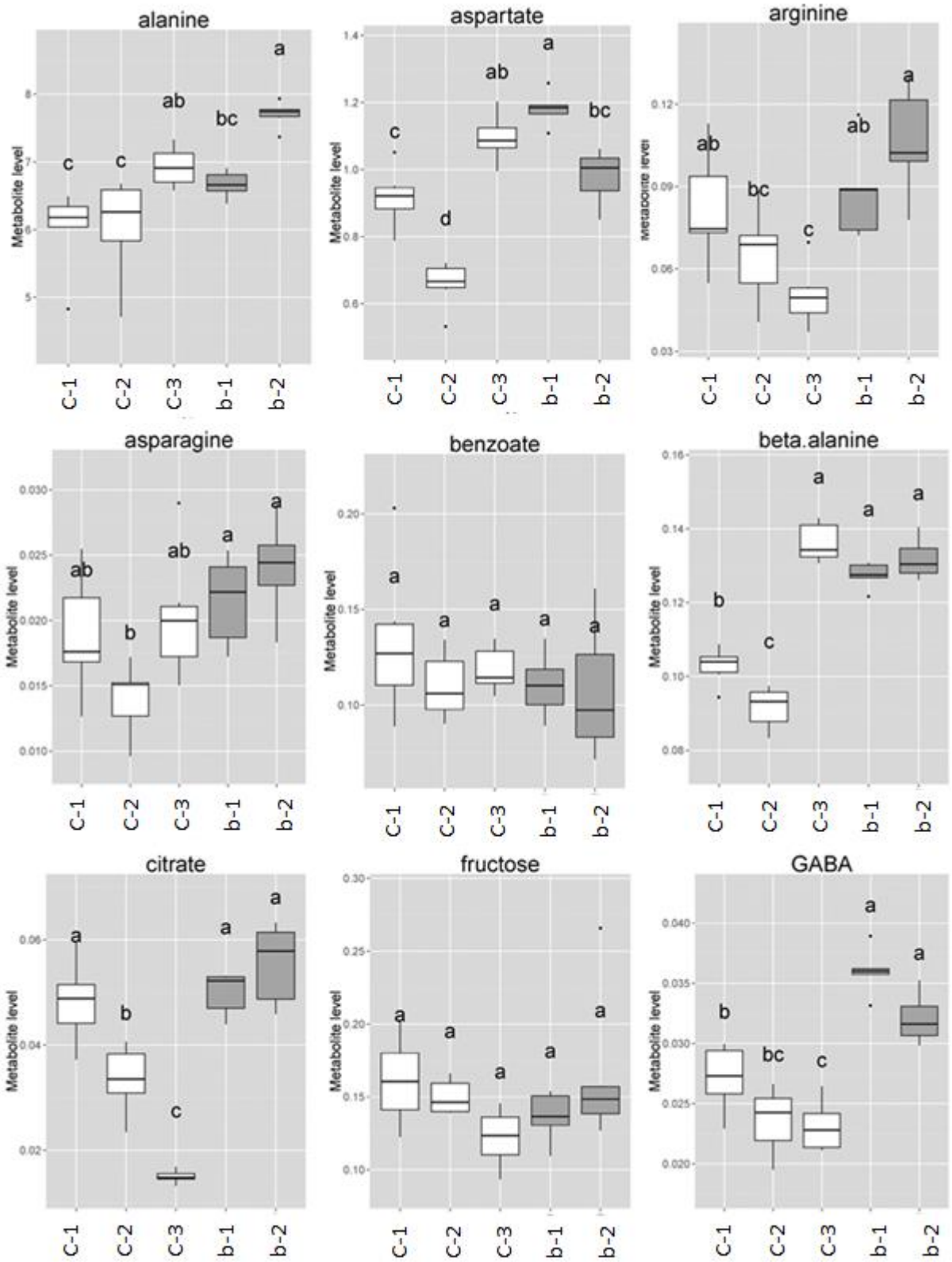
alanine
aspartate
arginine
asparagine
benzoate
beta.alanine
citrate
fructose
GABA
Metabolite level
C-1
C-2
C-3
b-1
b-2

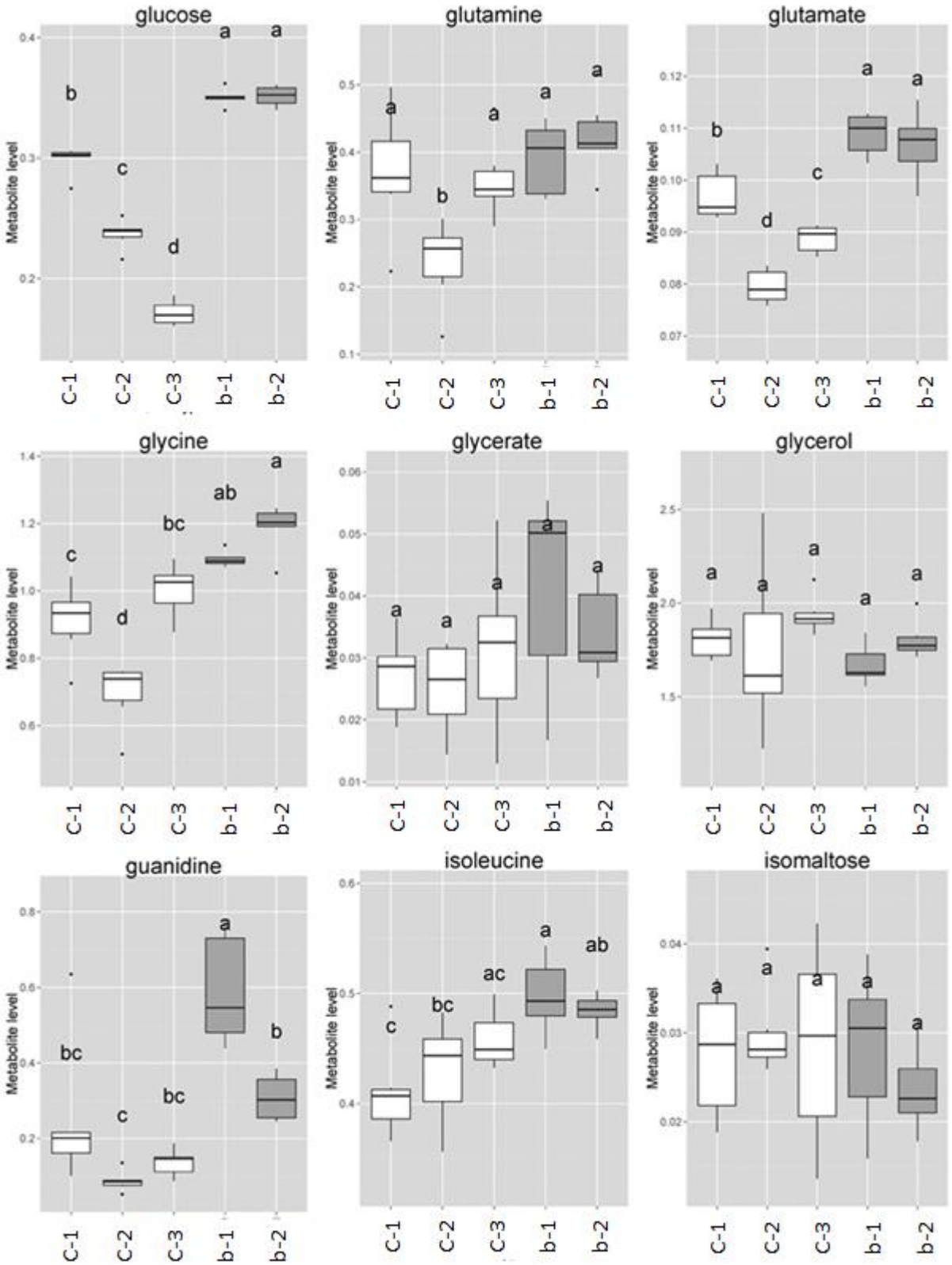
glucose
glutamine
glutamate
glycine
glycerate
glycerol
guanidine
isoleucine
isomaltose
Metabolite level
C-1
C-2
C-3
b-1
b-2

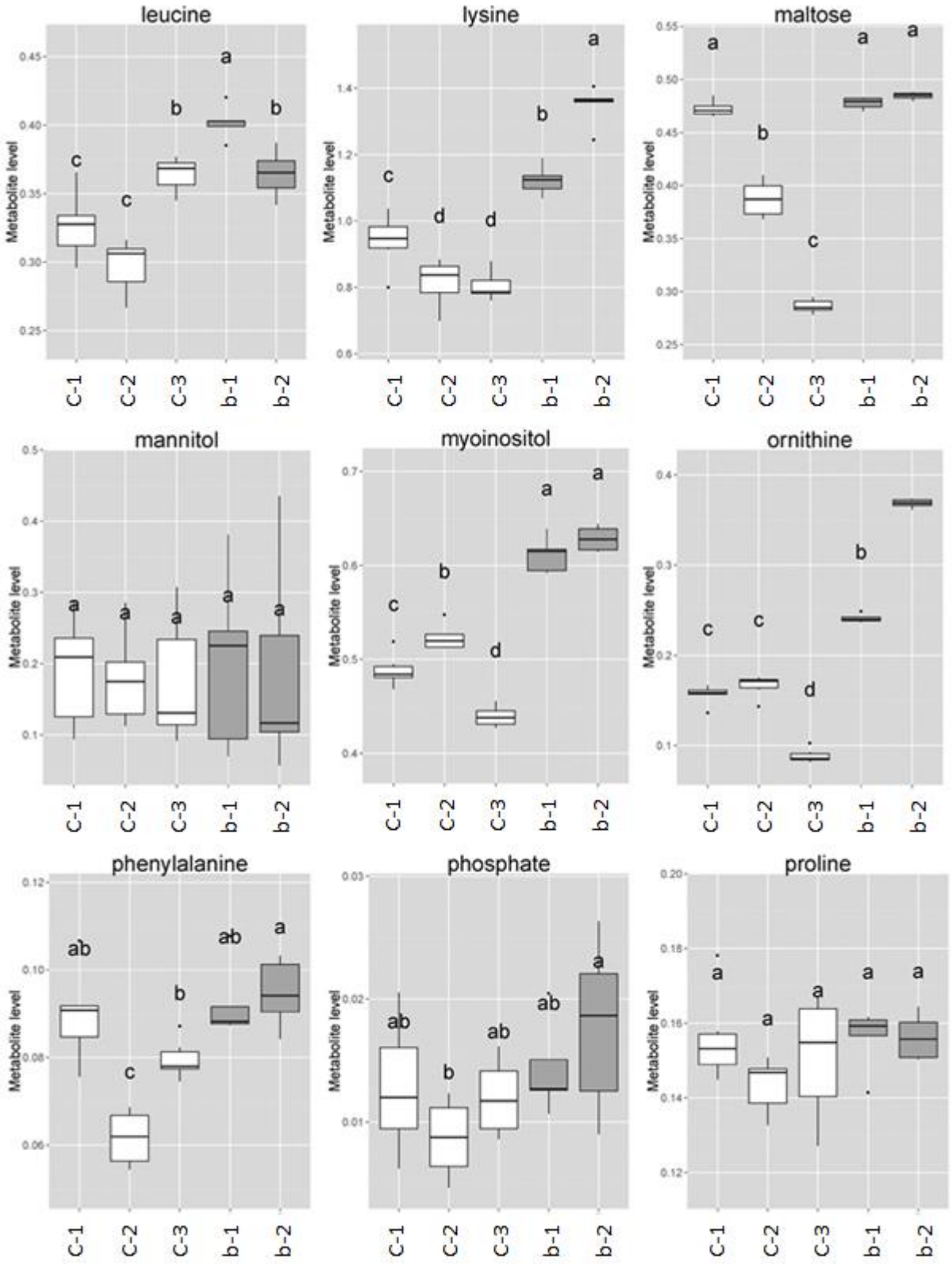
leucine
lysine
maltose
mannitol
myoinositol
ornithine
phenylalanine
phosphate
proline
Metabolite level
C-1
C-2
C-3
b-1
b-2

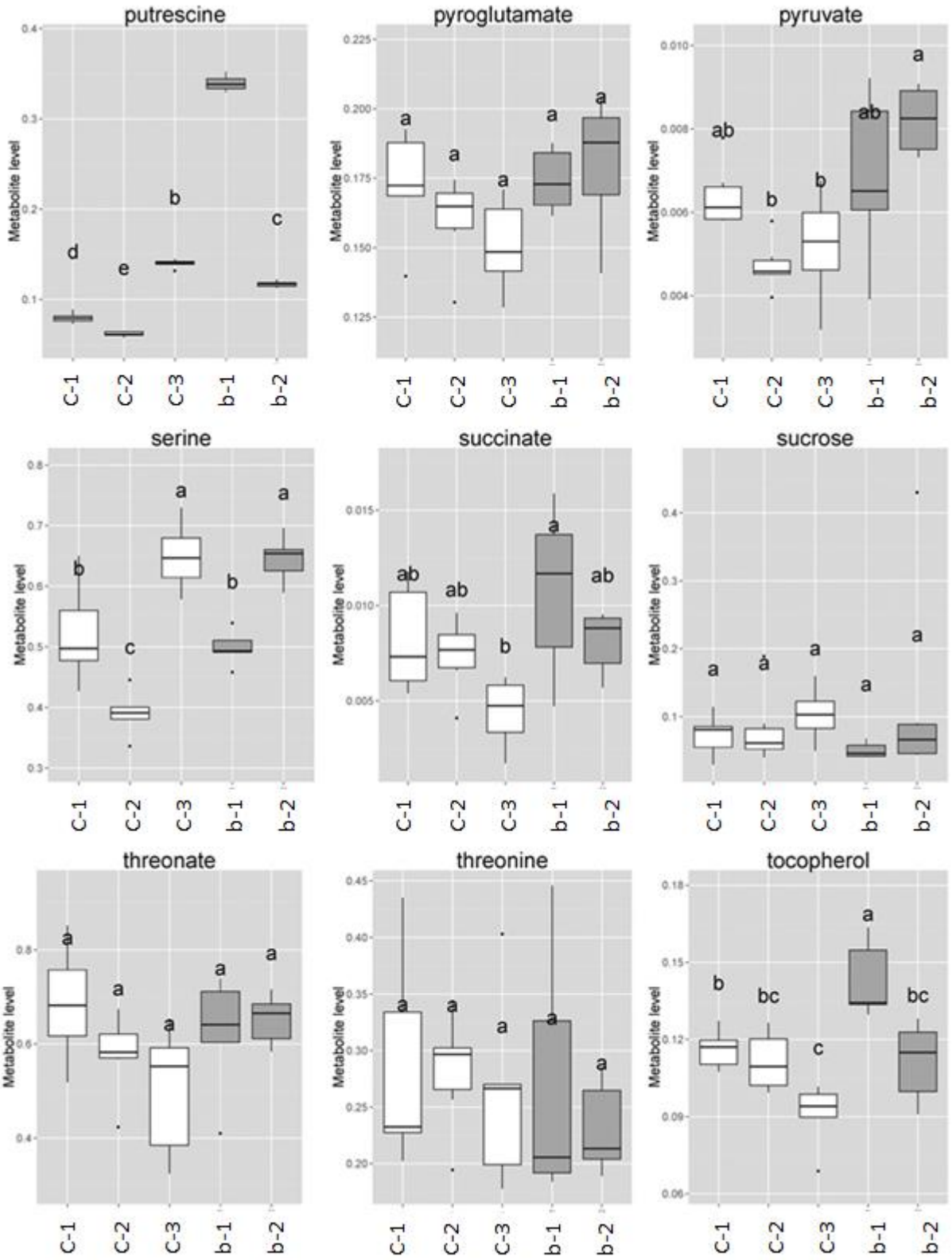
putrescine
pyroglutamate
pyruvate
serine
succinate
sucrose
threonate
threonine
tocopherol
Metabolite level
C-1
C-2
C-3
b-1
b-2

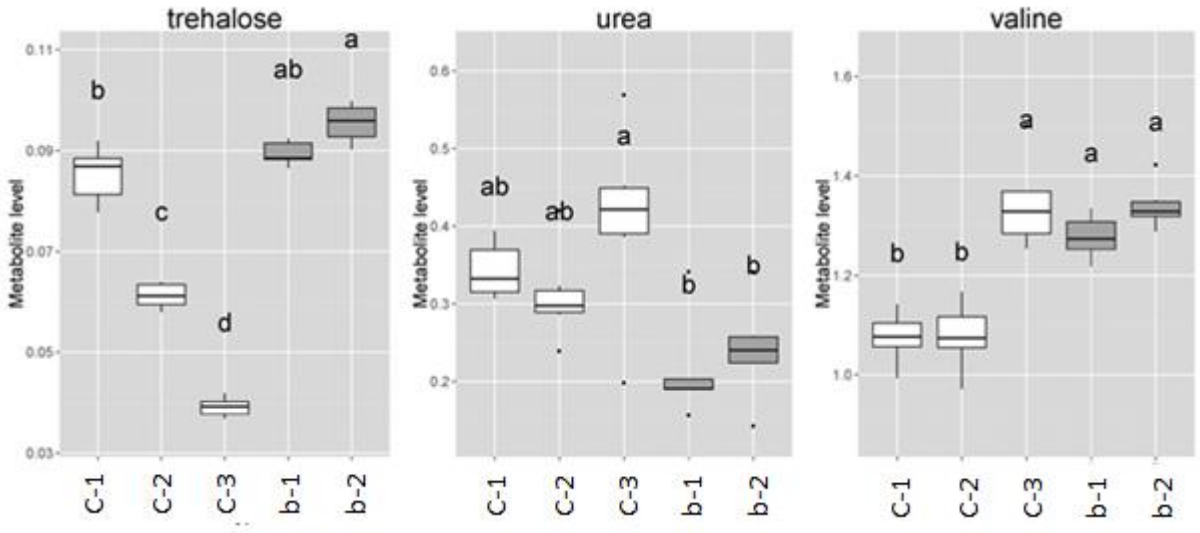

Appendix Figure S9. Metabolite profiling of *bZIP14* overexpression lines. White and grey box plots show relative metabolite levels in the three control lines (from left to right C-1 to C-3) and two *bZIP14* overexpressing lines (from left to right b-1 and b-2). Letters indicate the results of a Tukey's test comparing metabolite levels amongst genotypes (n=6).

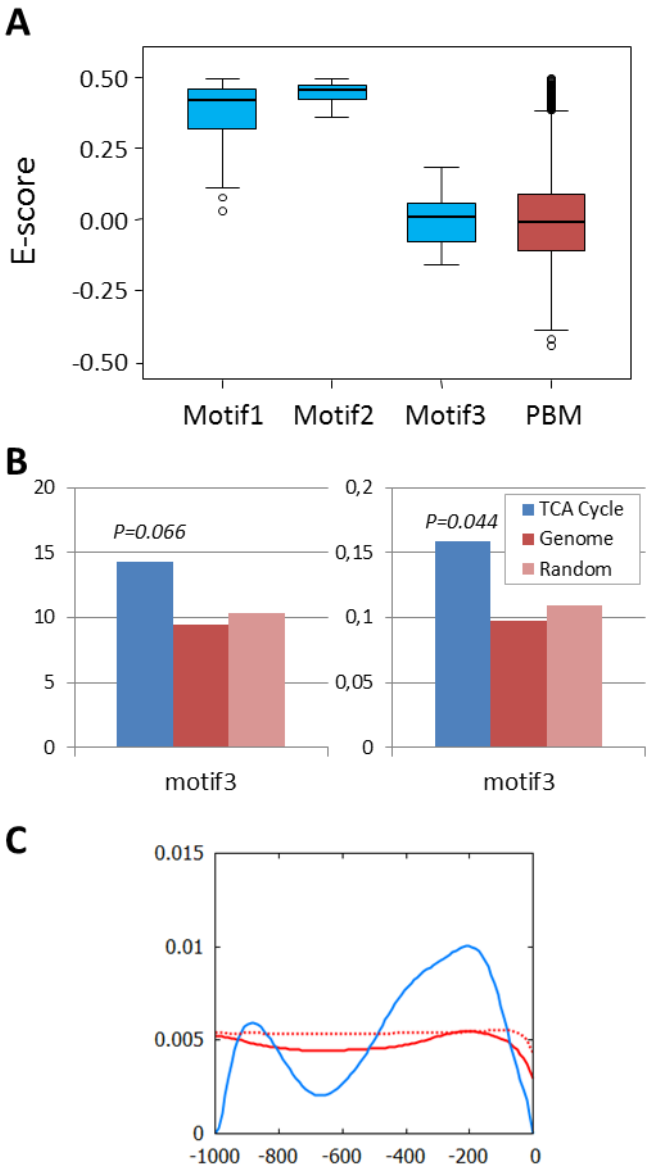

Appendix Figure S10. bZIP14 does not bind the CACGTG motif.

A E-score distributions of motif 1 (sequence TGACGT), motif 2 (GTACGTA) and motif 3 (CACGTG) as determined in the protein binding array assay. The distribution of E-scores of all possible sequences represented in the protein binding microarray is shown in red.

B Scan for motif 3 in all *P. tricornutum* gene promoters (genome in red; random promoters in light red) or only those linked with the TCA cycle (in blue). Left and right panels show the % promoters with motif 3 and the number of motifs per promoter, respectively, within 0.5 kb upstream of the ORF.

C Histogramme showing the density of motif 3 in the proximal promoter regions of the 'TCA cycle genes' (in blue), in the whole genome (in red) or in random promoters (dashed red). The complete scan of 1.0 kb upstream of the ORF is shown.

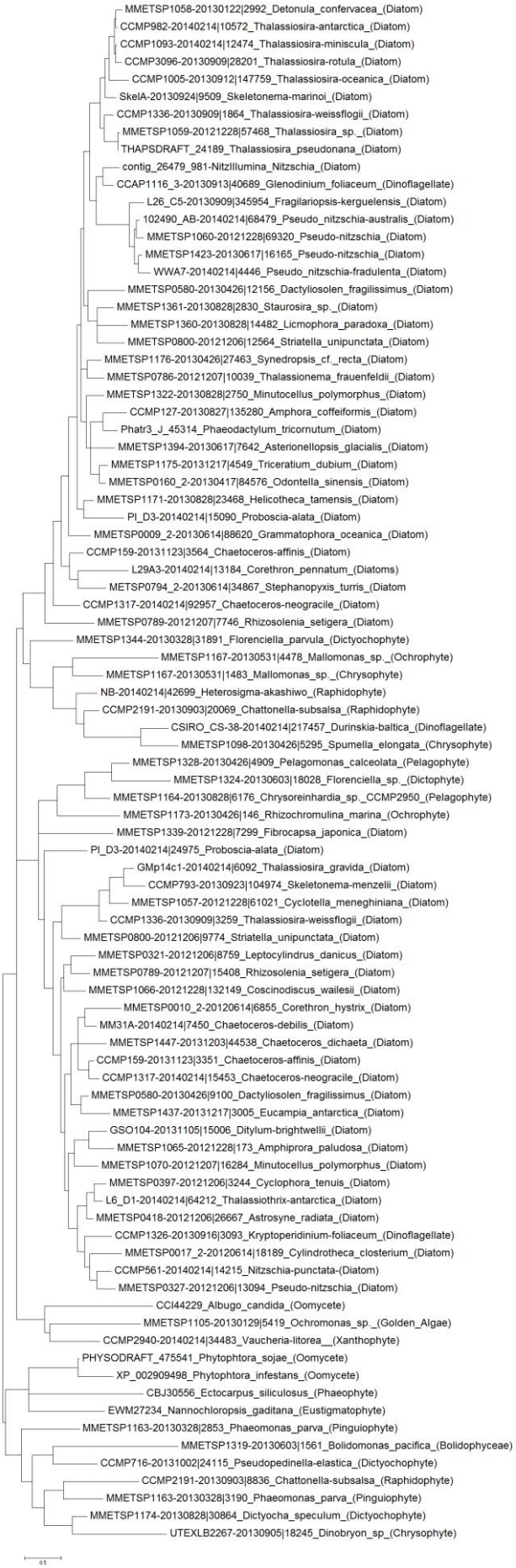
MMETSP1058-20130122|2992_Detonula_confervacea_(Diatom)
CCMP982-20140214|10572_Thalassiosira-antarctica_(Diatom)
CCMP1093-20140214|12474_Thalassiosira-miniscula_(Diatom)
CCMP3096-20130909|28201_Thalassiosira-rotula_(Diatom)
CCMP1005-20130912|147759_Thalassiosira-oceanica_(Diatom)
SkelA-20130924|9509_Skeletonema-marinoi_(Diatom)
CCMP1336-20130909|1864_Thalassiosira-weissflogii_(Diatom)
MMETSP1059-20121228|57468_Thalassiosira_sp._(Diatom)
THAPSDRAFT_24189_Thalassiosira_pseudonana_(Diatom)
contig_26479_981-NitzIllumina_Nitzschia_(Diatom)
CCAP1116_3-20130913|40689_Glenodinium_foliaceum_(Dinoflagellate)
L26_C5-20130909|345954_Fragilariopsis-kerguelensis_(Diatom)
102490_AB-20140214|68479_Pseudo_nitzschia-australis_(Diatom)
MMETSP1060-20121228|69320_Pseudo-nitzschia_(Diatom)
MMETSP1423-20130617|16165_Pseudo-nitzschia_(Diatom)
WWA7-20140214|4446_Pseudo_nitzschia-fradulenta_(Diatom)
MMETSP0580-20130426|12156_Dactyliosolen_fragilissimus_(Diatom)
MMETSP1361-20130828|2830_Staurosira_sp._(Diatom)
MMETSP1360-20130828|14482_Licmophora_paradoxa_(Diatom)
MMETSP0800-20121206|12564_Striatella_unipunctata_(Diatom)
MMETSP1176-20130426|27463_Synedropsis_cf._recta_(Diatom)
MMETSP0786-20121207|10039_Thalassionema_frauenfeldii_(Diatom)
MMETSP1322-20130828|2750_Minutocellus_polymorphus_(Diatom)
CCMP127-20130827|135280_Amphora_coffeiformis_(Diatom)
Phatr3_J_45314_Phaeodactylum_tricornutum_(Diatom)
MMETSP1394-20130617|7642_Asterionellopsis_glacialis_(Diatom)
MMETSP1175-20131217|4549_Triceratium_dubium_(Diatom)
MMETSP0160_2-20130417|84576_Odontella_sinensis_(Diatom)
MMETSP1171-20130828|23468_Helicotheca_tamensis_(Diatom)
PI_D3-20140214|15090_Proboscia-alata_(Diatom)
MMETSP0009_2-20130614|88620_Grammatophora_oceanica_(Diatom)
CCMP159-20131123|3564_Chaetoceros-affinis_(Diatom)
L29A3-20140214|13184_Corethron_pennatum_(Diatoms)
METSP0794_2-20130614|34867_Stephanopyxis_turris_(Diatom
CCMP1317-20140214|92957_Chaetoceros-neogracile_(Diatom)
MMETSP0789-20121207|7746_Rhizosolenia_setigera_(Diatom)
MMETSP1344-20130328|31891_Florenciella_parvula_(Dictyochophyte)
MMETSP1167-20130531|4478_Mallomonas_sp._(Ochrophyte)
MMETSP1167-20130531|1483_Mallomonas_sp._(Chrysophyte)
NB-20140214|42699_Heterosigma-akashiwo_(Raphidophyte)
CCMP2191-20130903|20069_Chattonella-subsalsa_(Raphidophyte)
CSIRO_CS-38-20140214|217457_Durinskia-baltica_(Dinoflagellate)
MMETSP1098-20130426|5295_Spumella_elongata_(Chrysophyte)
MMETSP1328-20130426|4909_Pelagomonas_calceolata_(Pelagophyte)
MMETSP1324-20130603|18028_Florenciella_sp._(Dictophyte)
MMETSP1164-20130828|6176_Chrysoreinhardia_sp._CCMP2950_(Pelagophyte)
MMETSP1173-20130426|146_Rhizochromulina_marina_(Ochrophyte)
MMETSP1339-20121228|7299_Fibrocapsa_japonica_(Diatom)
PI_D3-20140214|24975_Proboscia-alata_(Diatom)
GMp14c1-20140214|6092_Thalassiosira_gravida_(Diatom)
CCMP793-20130923|104974_Skeletonema-menzelii_(Diatom)
MMETSP1057-20121228|61021_Cyclotella_meneghiniana_(Diatom)
CCMP1336-20130909|3259_Thalassiosira-weissflogii_(Diatom)
MMETSP0800-20121206|9774_Striatella_unipunctata_(Diatom)
MMETSP0321-20121206|8759_Leptocylindrus_danicus_(Diatom)
MMETSP0789-20121207|15408_Rhizosolenia_setigera_(Diatom)
MMETSP1066-20121228|132149_Coscinodiscus_wailesii_(Diatom)
MMETSP0010_2-20120614|6855_Corethron_hystrix_(Diatom)
MM31A-20140214|7450_Chaetoceros-debilis_(Diatom)
MMETSP1447-20131203|44538_Chaetoceros_dichaeta_(Diatom)
CCMP159-20131123|3351_Chaetoceros-affinis_(Diatom)
CCMP1317-20140214|15453_Chaetoceros-neogracile_(Diatom)
MMETSP0580-20130426|9100_Dactyliosolen_fragilissimus_(Diatom)
MMETSP1437-20131217|3005_Eucampia_antarctica_(Diatom)
GSO104-20131105|15006_Ditylum-brightwellii_(Diatom)
MMETSP1065-20121228|173_Amphiprora_paludosa_(Diatom)
MMETSP1070-20121207|16284_Minutocellus_polymorphus_(Diatom)
MMETSP0397-20121206|3244_Cyclophora_tenuis_(Diatom)
L6_D1-20140214|64212_Thalassiothrix-antarctica_(Diatom)
MMETSP0418-20121206|26667_Astrosyne_radiata_(Diatom)
CCMP1326-20130916|3093_Kryptoperidinium-foliaceum_(Dinoflagellate)
MMETSP0017_2-20120614|18189_Cylindrotheca_closterium_(Diatom)
CCMP561-20140214|14215_Nitzschia-punctata-(Diatom)
MMETSP0327-20121206|13094_Pseudo-nitzschia_(Diatom)
CCI44229_Albugo_candida_(Oomycete)
MMETSP1105-20130129|5419_Ochromonas_sp._(Golden_Algae)
CCMP2940-20140214|34483_Vaucheria-litorea__(Xanthophyte)
PHYSODRAFT_475541_Phytophtora_sojae_(Oomycete)
XP_002909498_Phytophtora_infestans_(Oomycete)
CBJ30556_Ectocarpus_siliculosus_(Phaeophyte)
EWM27234_Nannochloropsis_gaditana_(Eustigmatophyte)
MMETSP1163-20130328|2853_Phaeomonas_parva_(Pinguiophyte)
MMETSP1319-20130603|1561_Bolidomonas_pacifica_(Bolidophyceae)
CCMP716-20131002|24115_Pseudopedinella-elastica_(Dictyochophyte)
CCMP2191-20130903|8836_Chattonella-subsalsa_(Raphidophyte)
MMETSP1163-20130328|3190_Phaeomonas_parva_(Pinguiophyte)
MMETSP1174-20130828|30864_Dictyocha_speculum_(Dictyochophyte)
UTEXLB2267-20130905|18245_Dinobryon_sp_(Chrysophyte)
0.5

Appendix Figure S11. Molecular phylogenetic analysis by the maximum likelihood method. Sequences were retrieved by blasting the MMETSP database and the NCBI NR database. The retrieved sequences were selected to be representative and were aligned using the MUSCLE programme as implemented in MEGA7 using standard settings. The evolutionary history was inferred using the maximum likelihood method based on the JTT matrix-based model (Jones *et al*, 1992). The tree with the highest log likelihood (-7321.4631) is shown. Initial tree(s) for the heuristic search were obtained automatically by applying Neighbour-Join and BioNJ algorithms to a matrix of pairwise distances estimated using a JTT model, and then selecting the topology with superior log likelihood value. The tree is drawn to scale, with branch lengths measured in the number of substitutions per site. The analysis involved 88 amino acid sequences. All positions containing gaps and missing data were eliminated. There were a total of 51 positions in the final dataset. Evolutionary analyses were conducted in MEGA7.0.20 using standard settings (Kumar *et al*, 2016).

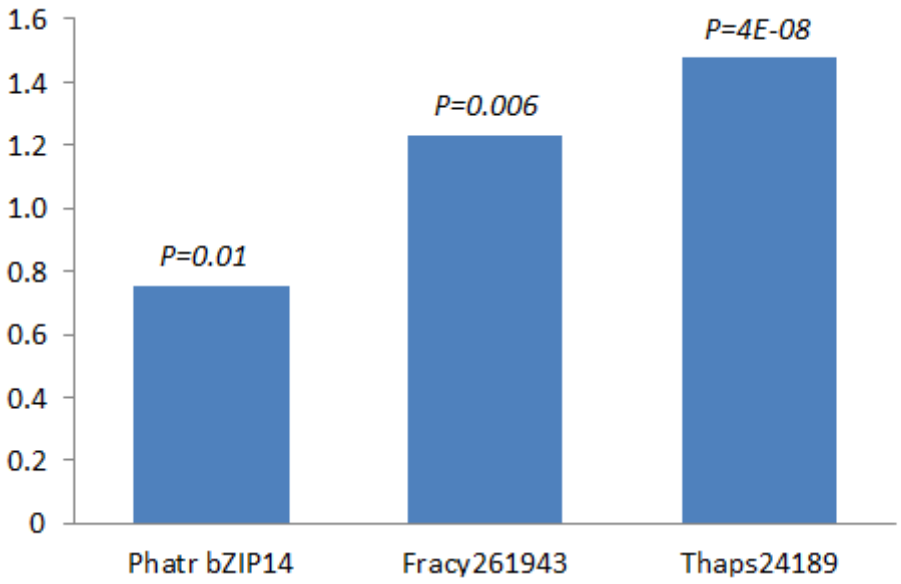

Appendix Figure S12. Expression analysis of *bZIP14* genes in *P. tricornutum*, *T. pseudonana* and *F. cylindrus* following nutrient starvation. For *P. tricornutum*, the data were derived from this study (nitrogen starvation after 20 h), for the two other species, expression data were collected from GEO GSE56132. Values in the *y*-axis indicate $\log_2$ fold change in nitrogen-starved versus nutrient-replete conditions (n=3). *P*-values were obtained from Cuffdiff (for *P. tricornutum*) and EdgeR (for the two other species), respectively.

Appendix Table S1. *P. tricornutum* gene promoters containing the predicted bZIP14 DNA-binding motifs. Promoter regions of 1 kb upstream of the start codon were scanned for the occurrence of the two motifs with a core ACGT sequence, namely TGACGT (motif 1) and GTACGTA (motif 2).

GENE	ANNOTATION	PROCESS	# MOTIF1	# MOTIF2
PHATR3_J22404	Pyruvate kinase {ECO:0000256|RuleBase:RU000504} [Source:Uniprot/SPTREMBL;Acc:B7G6Z9]	glycolytic process	6	0
PHATR3_J14284	Pyrophosphate-dependent phosphofructose kinase {ECO:0000313|EMBL:EEC46626.1} [Source:Uniprot/SPTREMBL;Acc:B7G4J8]	glycolytic process	1	2
PHATR3_J14792	Phosphoglycerate kinase {ECO:0000256|RuleBase:RU000532} [Source:Uniprot/SPTREMBL;Acc:B7G6H0]	glycolytic process	2	2
PHATR3_J22122	Glyceraldehyde-3-phosphate dehydrogenase {ECO:0000256|RuleBase:RU361160} [Source:Uniprot/SPTREMBL;Acc:B7G5Q1]	glycolytic process	3	1
PHATR3_J29014	Cytosolic class II aldolase {ECO:0000313|EMBL:EEC46498.1} [Source:Uniprot/SPTREMBL;Acc:B7G4R3]	glycolytic process	3	1
PHATR3_J22993	Fructose-1,6-bisphosphate aldolase {ECO:0000313|EMBL:EEC44953.1} [Source:Uniprot/SPTREMBL;Acc:B7G9G9]	glycolytic process	0	3
PHATR3_J42398	Malate dehydrogenase	malate metabolic process	1	2
PHATR3_J25308	Triosephosphate isomerase/glyceraldehyde-3-phosphate dehydrogenase {ECO:0000313|EMBL:EEC50801.1} [Source:Uniprot/SPTREMBL;Acc:B7FSI3]	glycolytic process	1	1
PHATR3_J32747	Glyceraldehyde-3-phosphate dehydrogenase {ECO:0000256|RuleBase:RU361160} [Source:Uniprot/SPTREMBL;Acc:B7FSI4]	glycolytic process	3	1
PHATR3_J41423	Fructose-bisphosphate aldolase {ECO:0000256|RuleBase:RU003994} [Source:Uniprot/SPTREMBL;Acc:B7GE67]	glycolytic process	2	1
PHATR3_J18228	Triosephosphate isomerase {ECO:0000256|RuleBase:RU000517} [Source:Uniprot/SPTREMBL;Acc:B7FSQ0]	glycolytic process	3	0
PHATR3_J52539	Succinate dehydrogenase [ubiquinone] iron-sulfur subunit, mitochondrial {ECO:0000256|RuleBase:RU361237} [Source:Uniprot/SPTREMBL;Acc:B7GA40]	tricarboxylic acid cycle	2	1
PHATR3_J11943	Phosphoglycerate mutase {ECO:0000256|RuleBase:RU004513} [Source:Uniprot/SPTREMBL;Acc:B7FXR4]	glycolytic process	0	1
PHATR3_J16722	Glucose-6-phosphate isomerase {ECO:0000256|RuleBase:RU000612} [Source:Uniprot/SPTREMBL;Acc:B7GDL0]	glycolytic process	0	1
PHATR3_J48983	Phosphoglycerate kinase {ECO:0000256|RuleBase:RU000532} [Source:Uniprot/SPTREMBL;Acc:B7G938]	glycolytic process	2	0
PHATR3_J51970	Malic enzyme {ECO:0000256|RuleBase:RU003426} [Source:Uniprot/SPTREMBL;Acc:B7FZD7]	malate metabolic process	0	1

GENE	ANNOTATION	PROCESS	# MOTIF1	# MOTIF2
PHATR3_J54082	Malic enzyme	malate metabolic process	2	0
PHATR3_J54738	Triosephosphate isomerase {ECO:0000256|RuleBase:RU000517} [Source:Uniprot/SPTREMBL;Acc:B7G3C1]	glycolytic process	2	0
PHATR3_J55126	PFP pyrophosphate dependent phosphofructokinase {ECO:0000313|EMBL:EEC43866.1} [Source:Uniprot/SPTREMBL;Acc:B7GCG9]	glycolytic process	0	2
PHATR3_J27976	Predicted protein {ECO:0000313|EMBL:EEC47679.1} [Source:Uniprot/SPTREMBL;Acc:B7G1G6]	tricarboxylic acid cycle	2	0
PHATR3_J29157	Phosphoglycerate kinase {ECO:0000256|RuleBase:RU000532} [Source:Uniprot/SPTREMBL;Acc:B7G5G4]	glycolytic process	2	0
PHATR3_J5629	Phosphoglycerate mutase {ECO:0000256|RuleBase:RU004513} [Source:Uniprot/SPTREMBL;Acc:B5Y4E3]	glycolytic process	1	1
PHATR3_J5857	glucose-6-phosphate isomerase	glycolytic process	1	1
PHATR3_EG00092	Pyrophosphate-dependent phosphofructose kinase {ECO:0000313|EMBL:EEC43176.1} [Source:Uniprot/SPTREMBL;Acc:B7GE27]	glycolytic process	0	1
PHATR3_EG02208	Glucose-6-phosphate isomerase {ECO:0000256|RuleBase:RU000612} [Source:Uniprot/SPTREMBL;Acc:B7GDV0]	glycolytic process	2	0
PHATR3_J41812	Succinate dehydrogenase flavoprotein {ECO:0000313|EMBL:ACI65968.1} [Source:Uniprot/SPTREMBL;Acc:B5Y5N6]	tricarboxylic acid cycle	1	0
PHATR3_J42447	Cytosolic aldolase {ECO:0000313|EMBL:EEC50983.1} [Source:Uniprot/SPTREMBL;Acc:B7FRC1]	glycolytic process	1	0
PHATR3_J49098	Pyruvate kinase {ECO:0000256|RuleBase:RU000504} [Source:Uniprot/SPTREMBL;Acc:B7G9H4]	glycolytic process	1	0
PHATR3_J51404	Phosphoglycerate mutase {ECO:0000256|RuleBase:RU004513} [Source:Uniprot/SPTREMBL;Acc:B7FPT5]	glycolytic process	0	1
PHATR3_J55035	Pyruvate dehydrogenase E1 component subunit alpha {ECO:0000256|RuleBase:RU361139} [Source:Uniprot/SPTREMBL;Acc:B7GAB0]	glycolytic process	2	0
PHATR3_J5605	PGAM_5	glycolytic process	1	0
PHATR3_J8982	PGAM_2	glycolytic process	1	0
PHATR3_EG02261	Putative phosphoenolpyruvate carboxylase {ECO:0000313|EMBL:BAK09353.1} [Source:Uniprot/SPTREMBL;Acc:F1SXA1]	tricarboxylic acid cycle	1	0
PHATR3_J22913	Pyruvate kinase {ECO:0000256|RuleBase:RU000504} [Source:Uniprot/SPTREMBL;Acc:B7G961]	glycolytic process	1	0
PHATR3_J23924	Glucose-6-phosphate isomerase {ECO:0000256|RuleBase:RU000612} [Source:Uniprot/SPTREMBL;Acc:B7GDK9]	glycolytic process	0	1
PHATR3_J26290	aconitate hydratase 2	tricarboxylic acid cycle	0	1
PHATR3_J54998	Pyruvate kinase {ECO:0000256|RuleBase:RU000504} [Source:Uniprot/SPTREMBL;Acc:B7G9G7]	glycolytic process	1	0

GENE	ANNOTATION	PROCESS	# MOTIF1	# MOTIF2
PHATR3_J55079	Pyruvate kinase {ECO:0000256|RuleBase:RU000504} [Source:Uniprot/SPTREMBL;Acc:B7GBB9]	glycolytic process	1	0
PHATR3_J54834	Malate dehydrogenase.	tricarboxylic acid cycle	1	0
PHATR3_J20934	Malate dehydrogenase	tricarboxylic acid cycle	2	0
PHATR3_J42015	succinate-CoA ligase (SCSCa)	tricarboxylic acid cycle	2	0
PHATR3_J26921	Suc SYN	tricarboxylic acid cycle	3	0
PHATR2_45314	bZIP14	Transcription factor	1	0

Appendix Table S2. Parameters used for peak annotation in the GC-MS analysis. Indicated are: Peak no., compound number referenced back to the main text; RT, expected retention time; TTI, tag time index; TD, time deviation; Putative metabolite/derivative name, putative identification of the metabolite/derivative; Literature name, corresponding metabolite name in literature; MF, molecular formula of the metabolite or its FA adduct; m/z, mass to charge ratio. All identifications are level A, by standard or NMR.

Peak no.	RT	TTI	TD	Putative metabolite/derivative name	Literature name	MF	m/z
1	531145	529987	-0,27	M000011_A164001-101_METB_531145_TOF_Phenylalanine, DL- (2TMS)	phenylalanine	C9H11NO2	218
2	790560	788911	-0,15	M000012_A223001-101_METB_790560_TOF_Tryptophan, L- (3TMS)	tryptophan	C11H12N2O2	202
3	550100	549493	-0,05	M000013_A168001-101_METB_550100_TOF_Asparagine, DL- (3TMS)	asparagine	C4H8N2O3	231
4	615467	615003	0,03	M000014_A192003-101_METB_615467_TOF_Lysine, L- (4TMS)	lysine	C6H14N2O2	174
5	357523	356928	-0,15	M000015_A138001-101_METB_357523_TOF_Serine, DL- (3TMS)	serine	C3H7NO3	204
6	368365	369080	0,19	M000016_A140001-101_METB_368365_TOF_Threonine, DL- (3TMS)	threonine	C4H9NO3	117
7	319193	318893	-0,08	M000017_A132002-101_METB_319193_TOF_Isoleucine, L- (2TMS)	isoleucine	C6H13NO2	158
8	305020	304918	-0,03	M000025_A129002-101_METB_301020_TOF_Leucine, DL- (2TMS)	leucine	C6H13NO2	158
9	208565	208741	-0,01	M000026_A110001-101_METB_208565_TOF_Alanine, DL- (2TMS)	alanine	C3H7NO2	116
10	394250	393887	-0,08	M000027_A144001-101_METB_394250_TOF_Alanine, beta- (3TMS)	beta-alanine	C3H7NO2	174
11	570427	570440	0,02	M000028_A182002-101_METB-METB_570427_TOF_Ornithine, DL- (4TMS)	ornithine	C5H12N2O2	420
12	338693	339666	0,32	M000029_A132003-101_METB_338693_TOF_Proline, L- (2TMS)	proline	C5H9NO2	117
13	271580	271479	-0,03	M000030_A122001-101_METB_271580_TOF_Valine, DL- (2TMS)	valine	C5H11NO2	144
14	325180	324925	-0,11	M000031_A133001-101_METB_325180_TOF_Glycine (3TMS)	glycine	C2H5NO2	174
15	598300	597549	-0,08	M000032_A178001-101_METB_598300_TOF_Glutamine, DL- (3TMS)	glutamine	C5H10N2O3	156
16	457283	456619	-0,01	M000033_A152002-101_METB_457283_TOF_Aspartic acid, L- (3TMS)	aspartate	C4H7NO4	232
17	448453	447835	-0,09	M000034_A153001-101_METB_448453_TOF_Proline, 4-hydroxy-, DL-, trans- (3TMS)	4hydroxyproline	C5H9NO3	140
18	658337	655216	-0,46	M000035_A194002-101_METB_658337_TOF_Tyrosine, DL- (3TMS)	tyrosine	C9H11NO3	179
19	507780	507548	-0,09	M000036_A163001-101_METB_507780_TOF_Glutamic acid, DL- (3TMS)	glutamate	C5H9NO4	363
20	506483	505285	0,16	M000037_A153002-101_METB-METB_506483_TOF_Pyroglutamic acid, DL- (2TMS)	pyroglutamate	C5H7NO3	258
21	605940	605094	-0,14	M000038_A183001-101_METB-METB_605940_TOF_Arginine, DL-, -NH3 (3TMS)	arginine	C6H11N3O2	157

Peak no.	RT	TTI	TD	Putative metabolite/derivative name	Literature name	MF	m/z
22	598880	597918	-0,18	M000040_A191001-101_METB-METB_598880_TOF_Glucose, D- (1MEOX) (5TMS)	glucose	C6H12O6	160
23	840783	839645	-0,14	M000044_A264001-101_METB_840783_TOF_Sucrose, D- (8TMS)	sucrose	C12H22O11	361
24	870355	869731	-0,06	M000048_A274001-101_METB_870355_TOF_Maltose, D- (1MEOX) (8TMS)	maltose	C12H22O11	160
25	291783	291885	-0,02	M000053_A129003-101_METB_291783_TOF_Glycerol (3TMS)	glycerol	C3H8O3	117
26	499920	498883	-0,07	M000057_A171001-101_METB_499920_TOF_Xylitol (5TMS)	xylitol	C5H12O5	205
27	653910	653731	-0,03	M000060_A209002-101_METB_653910_TOF_Inositol, myo (6TMS)	myoinositol	C6H12O6	191
28	371255	371077	-0,06	M000067_A137001-101_METB_371255_TOF_Fumaric acid (2TMS)	fumarate	C4H4O4	245
29	592883	591419	-0,27	M000069_A182004-101_METB-METB_592883_TOF_Citric acid (4TMS)	citrate	C6H8O7	273
30	222650	222521	-0,08	M000071_A104002-101_METB_222650_TOF_Pyruvic acid (1MEOX) (1TMS)	pyruvate	C3H4O3	174
31	345050	344114	-0,27	M000073_A135003-101_METB_345050_TOF_Glyceric acid, DL- (3TMS)	glycerate	C3H6O4	189
32	365427	364755	0,14	M000074_A134001-101_METB_365427_TOF_Succinic acid (2TMS)	succinate	C4H6O4	247
33	333520	333190	-0,12	M000075_A129001-101_METB_333520_TOF_Phosphoric acid (3TMS)	phosphate	H3O4P	299
34	458330	457574	-0,24	M000078_A156001-101_METB_458330_TOF_Threonic acid (4TMS)	threonate	C4H8O5	292
35	624990	623620	-0,22	M000082_A185002-101_METB-METB_624990_TOF_Dehydroascorbic acid dimer (TMS)	dehydroascorbate	C6H6O6	173
36	190250	190658	0,27	M000100_A105001-101_CONT-METB_190250_TOF_Lactic acid, DL- (2TMS)	lactate	C3H6O3	219
37	917000	915437	-0,17	M000107_A291002-101_METB_917000_TOF_Isomaltose (1MEOX) (8TMS)	isomaltose	C12H22O11	361
38	452200	451803	-0,04	M000114_A153003-101_METB_452200_TOF_Butyric acid, 4-amino- (3TMS)	GABA	C4H9NO2	304
39	517180	517114	0,02	M000186_A175002-101_METB-METB_517180_TOF_Putrescine (4TMS)	putrescine	C4H12N2	174
40	1081300	1077515	-0,34	M000269_A355003-101_METB_1081300_TOF_Maltotriose 11TMS/1MeOx BP	maltotriose	C18H32O16	217
41	348220	347878	-0,09	M000347_A128003-101_CONT-METB_348220_TOF_Benzoic acid (1TMS)	benzoate	C7H6O2	105
42	340357	340516	-0,17	M000364_A127002-101_METB_340357_TOF_Urea (2TMS)	urea	CH4N2O	171
43	266760	265927	-0,34	M000435_A116009-101_MST_266760_TOF_Guanidine (3TMS)	guanidine		146
44	206867	207359	0,34	M000517_A106002-101_CONT-MST_206867_TOF_Glycolic acid (2TMS)	glycolate	C2H4O3	177
45	523847	522703	-0,22	M000571_A158004-101_METB_523847_TOF_Glutaric acid, 2-oxo- (1MEOX) (2TMS)	2OG	C5H6O5	304
46	498150	497860	-0,12	M000579_A166001-101_METB_498150_TOF_Xylose, D- (1MEOX) (4TMS)	xylose/lyxose	C5H10O5	160
47	626890	629308	0,42	M000596_A199002-101_METB_626890_TOF_Galactonic acid (6TMS)	galactonate	C6H12O7	157

Peak no.	RT	TTI	TD	Putative metabolite/derivative name	Literature name	MF	m/z
48	579380	578188	-0,24	M000606_A187002-101_METB_579380_TOF_Fructose, D- (1MEOX) (5TMS)	fructose	C6H12O6	217
49	1070600	1069783	-0,08	M000626_A316001-101_METB_1070600_TOF_Tocopherol, alpha- (1TMS)	tocopherol	C29H50O2	237
50	618870	619535	0,02	M000639_A189003-101_METB_618870_TOF_Galactonic acid-1,4-lactone, D(-)- (4TMS)	galactonolactone	C6H10O6	217
51	876240	880218	0,49	M000671_A274002-101_METB_876240_TOF_Trehalose, alpha,alpha'-, D- (8TMS)	trehalose	C12H22O11	169
52	583850	581142	-0,37	M000687_A193002-101_METB_583850_TOF_Mannitol, D- (6TMS)	mannitol	C6H14O6	217
53	716750	716569	-0,02	M000709_A225006-101_METB_716750_TOF_Glucoheptonic acid (7TMS)	glucoheptonate		217

Appendix Table S3. Primers used for cloning and qRT-PCR analysis.

Primer	Sequence
For cloning	
FW_bZIP14_45314	5′-GGGGACAAGTTTGTACAAAAAAGCAGGCTCCATGCGATTTCCAGCCGCTTCAGTGG-3′
RV_bZIP14_45314	5′-GGGGACCACTTTGTACAAGAAAGCTGGGTCTCMCCAACCCACAGGGGCTGCAAGA-3′
FW_pJ41812_Y1H	5′-GGGGACAACTTTGTATAGAAAAGTTGAACATTCCTAAATCTCAAACGCCGATTCAC-3′
RV_pJ41812_Y1H	5′-GGGGACTGCTTTTTTGTACAAACTTGGCTTACAATCACGGATTTTCGTAGTTGGTTTAC-3′
FW_pJ52539_Y1H	5′-GGGGACAACTTTGTATAGAAAAGTTGAAGAGAGAGTGTTGGGATGAAGAACG-3′
RV_pJ52539_Y1H	5′-GGGGACTGCTTTTTTGTACAAACTTGGCAAGTGATTCCAGTTTGCCACGTC-3′
For qRT-PCR	
FW_Q_Bzip14	5′-AGAAATGGCCGAAATGTGTC-3′
RV_Q_Bzip14	5′-GAAGTTGGCTCGGACTCAAG-3′
FW_26290_Q_AH	5′-ACTGAAAGAACCCGTGTTGG-3′
RV_26290_Q_AH	5′-CGTCCATCTTGGTAGGAGGA-3′
FW_20934_Q_ICD	5′-TGGATTCGACATGAACCTGA-3′
RV_20934_Q_ICD	5′-TCTTTGCGCATTTTCAACAG-3′
FW_29016_Q_OGD	5′-CACATTTGGAATGCGTCAAC-3′
RV_29016_Q_OGD	5′-GTTGGTGGTGAAGCCAATCT-3′
FW_42015_Q_SCSa	5′-ATTAAACCCGGTGAATGCAA-3′
RV_42015_Q_SCSa	5′-GGTGAAACGTTCCAAGCAAT-3′
FW_26921_Q_SCSa2	5′-AAGCCATCCTCGTCAACATC-3′
RV_26921_Q_SCSa2	5′-GCATCTTCCAGATCCTCTGC-3′
FW_52539_Q_SDH2	5′-CGCTCGCCTGTCTATCCTAC-3′
RV_52539_Q_SDH2	5′-ATACATTCCGTCGAGCTTGG-3′
FW_18516_Q_SDHcb	5′-CGCTGTCGCCAGTATTACAA-3′
RV_18516_Q_SDHcb	5′-TCAAACCTCCCCCATAATGA-3′
FW_41812_Q_SDH1	5′-CCAACCAGGACAACGAGTTT-3′
RV_41812_Q_SDH1	5′-TGAAACGACGTCTCTCGATG-3′
FW_36139_Q_FUM	5′-ACGAGCGAACTCTACCAGGA-3′
RV_36139_Q_FUM	5′-CCCAAGGCTAAACGGTACAA-3′
FW_19708_Q_FUM1	5′-GGTTACCGGACTACGCAAAA-3′
RV_19708_Q_FUM1	5′-CTTTTTGCAAGCATTCGTCA-3′
FW_Q_Urease	5′-GACAGGATTCGGTTGCTGAT-3′
RV_Q_Urease	5′-GCCGAGACAGGGTTGTGTAT-3′
FW_Q_CS_30145	5′-TCCTGAAATGGATCCAGGAG-3′
RV_Q_CS_30145	5′-AAAATGTCGGGCATGACTTC-3′
FW_Q_MD_42398	5′-GGTAGCTGCGGATCTCAGTC-3′
RV_Q_MD_42398	5′-CAGCGTTGGTGTTGAAGAGA-3′
Q_M_FW_RP3A	5′-AAAGAGCATGCCAAGTGGTG-3′
Q_M_RV_RP3A	5′-TCTACAGCTCGAATGTCCCC-3′
Q_M_FW_PUA	5′-TGGATTGACAAACCCTGGC-3′
Q_M_RV_PUA	5′-TCCCCCTCACTTCCAAACTG-3′
Q_L_FW_VTC4	5′-GGCACATTTCGGCTACGATT-3′
Q_L_RV_VTC4	5′-TATCCTCGTGTACGTGTCCG-3′

Appendix References

Alipanah L, Rohloff J, Winge P, Bones AM, Brembu T (2015) Whole-cell response to nitrogen deprivation in the diatom *Phaeodactylum tricornutum*. *J Exp Bot* **66:** 6281-6296

Chauton MS, Winge P, Brembu T, Vadstein O, Bones AM (2013) Gene regulation of carbon fixation, storage and utilization in the diatom *Phaeodactylum tricornutum* acclimated to light/dark cycles. *Plant Physiol* **161:** 1034-1048

Daboussi F, Leduc S, Maréchal A, Dubois G, Guyot V, Perez-Michaut C, Amato A, Falciatore A, Juillerat A, Beurdeley M, Voytas DF, Cavarec L, Duchateau P (2014) Genome engineering empowers the diatom *Phaeodactylum tricornutum* for biotechnology. *Nat Commun* **5:** 3831

Falkowski PG, Katz ME, Knoll AH, Quigg A, Raven JA, Schofield O, Taylor FJR (2004) The evolution of modern eukaryotic phytoplankton. *Science* **305:** 354-360

Huysman MJJ, Fortunato AE, Matthijs M, Schellenberger Costa B, Vanderhaeghen R, Van den Daele H, Sachse M, Inzé D, Bowler C, Kroth PG, Wilhelm C, Falciatore A, Vyverman W, De Veylder L (2013) AUREOCHROME1a-mediated induction of the diatom-specific cyclin *dsCYC2* controls the onset of cell division in diatoms (*Phaeodactylum tricornutum*). *Plant Cell* **25:** 215-228

Jones DT, Taylor WR, Thornton JM (1992) The rapid generation of mutation data matrices from protein sequences. *Comput Biol Med* **8:** 275-282

Kumar S, Stecher G, Tamura K (2016) MEGA7: Molecular Evolutionary Genetics Analysis version 7.0 for bigger datasets. *Mol Biol Evol* **33:** 1870-1874

Levitan O, Dinamarca J, Zelzion E, Lun DS, Guerra LT, Kim MK, Kim J, Van Mooy BAS, Bhattacharya D, Falkowski PG (2015) Remodeling of intermediate metabolism in the diatom *Phaeodactylum tricornutum* under nitrogen stress. *Proc Natl Acad Sci USA* **112:** 412-417

Matthijs M, Fabris M, Broos S, Vyverman W, Goossens A (2016) Profiling of the early nitrogen stress response in the diatom *Phaeodactylum tricornutum* reveals a novel family of RING-domain transcription factors. *Plant Physiol* **170:** 489-498

Valenzuela J, Mazurie A, Carlson RP, Gerlach R, Cooksey KE, Peyton BM, Fields MW (2012) Potential role of multiple carbon fixation pathways during lipid accumulation in *Phaeodactylum tricornutum*. *Biotechnol Biofuels* **5:** 40

Yang Z-K, Niu Y-F, Ma Y-H, Xue J, Zhang M-H, Yang W-D, Liu J-S, Lu S-H, Guan Y, Li H-Y (2013) Molecular and cellular mechanisms of neutral lipid accumulation in diatom following nitrogen deprivation. *Biotechnol Biofuels* **6:** 67